

An experimental study on transporting a free-float capable tension leg platform for a 10 MW wind turbine in waves

Jordi Mas-Soler ^{a,b}, Emre Uzunoglu ^c, Gabriele Bulian ^d, C. Guedes Soares ^c,
Antonio Souto-Iglesias ^{e,*}

^a CEHINAV, ETSIN, Universidad Politécnica de Madrid (UPM), Madrid, Spain

^b TPN, Dept. of Naval Arch. & Ocean Eng. Escola Politécnica, University of São Paulo, São Paulo, Brazil

^c Centre for Marine Technology and Ocean Engineering (CENTEC), Instituto Superior Técnico, Universidade de Lisboa, Lisbon, Portugal

^d Department of Engineering and Architecture, University of Trieste, Via A. Valerio 10, 34127, Trieste, Italy

^e CEHINAV, DACSON, ETSIN, UPM, Madrid, Spain

ARTICLE INFO

Keywords:

Floating wind turbine (FWT)
Tension leg platform (TLP)
Negative added resistance in waves
Transport tests in waves
Bluff bodies

ABSTRACT

The paper presents the towing tests of CENTEC-TLP, a state-of-the-art free-float capable tension leg platform supporting a 10 MW wind turbine. The platform's design process and the overall dynamic behaviour was previously described in the literature. This work focuses on the platform's transportation stage, which is designed to have a shallow draft and certain characteristics resembling blunt bodies such as barges. The hydrodynamic behavior of this hull form in calm water and waves is investigated experimentally. The results are compared with similar relevant data available in the literature. As for added resistance in waves, the influence of wave characteristics and speed are evaluated. It is found that some of the cases display a reduction of average resistance in waves compared to calm water. Finally, the dynamic behaviour of the system in two relevant sea states is assessed with reference to risk of excessive motions during transport.

1. Introduction

There is a growing interest from the electric power generation sector in floating wind turbines (FWT) stemming from the large water depths characterising regions suitable for offshore wind energy generation in many European locations (e.g., the coast of Norway and the Mediterranean) and Japan. Thus, the current situation of the sector that is very much based on fixed bottom offshore wind in shallow water is expanding [1]. A series of recently launched units in a quasi-industrial scale confirms this interest and the ongoing process of moving to deeper waters, (see e.g. Equinor [2]; Rodrigues et al. [3]; Vieira et al. [4] and SBM Offshore [5].

For semi-submersibles and TLPs, towing to the installation site by standard tug boats is considered to be the most economical option. Using tugs reduces the operation costs significantly compared to specialized barges and large transport vessels such as the SAIPEM 7000 in Hywind [6] and Netherlands's Dockwise Shipping projects. Examples of towing manoeuvres with tugs are

the installation and decommissioning of the WindFloat platform (Fig. 1, left panel) and the towing of the Spanish ESTEYCO's ELICAN platform [7] (Fig. 1, right panel), using auxiliary floaters. Alternative approaches include the transport and installation of IBERDROLA's TLPWIND concept that is moved with a specialized barge [8,9] and GICON's TLP [10] that relies on a gravity anchor that is lowered when the structure reaches to position. These studies show the overall interest in towing processes with the tower and the turbine installed, which mostly relates to the difficulty in installing them offshore. Therefore, the methods of moving the structure into position with the turbine installed in dock are evaluated.

To cover these operations, it is desirable for engineers to know the motion dynamics and have an early estimate of the number and power of the tug units necessary to transport the turbines to the installation site. Along with the number of tugs, knowing the sea states in which the operation will be feasible with admissible risk of excessive motions is also necessary for the global cost estimation of the project. Kim and wan Kim [11] and Castro-Santos and Diaz-Casas [12] detail this type of cost estimation processes. It should also be noted that unlike the oil and gas sector where a single platform is sufficient for a chosen site, wind turbines are installed in

* Corresponding author.

E-mail address: antonio.souto@upm.es (A. Souto-Iglesias).



Fig. 1. Towing maneuver of WindFloat unit, left (credits to Recharge, Oslo, Norway) and ESTEYCO's ELICAN, right (credits to ESTEYCO).

arrays. Therefore, the tow operation needs to be repeated multiple times. Accordingly, having a good understanding of the towing operations becomes essential for the progression of offshore wind.

The next section provides an in-depth look at the recent developments in the topics introduced above. The following sections focus on the CENTEC-TLP. It is a free-float capable TLP (FTLP) for which the details, design methodology, and numerical motion dynamics are available in Refs. [13,14]. A summary of the floater and the turbine (i.e., DTU 10 MW [15]) precede the experimental setup and test matrices. Subsequently, the results regarding transportation dynamics and resistance in waves of this hull form are examined. An interesting aspect of the floater is that in some cases it displays a reduction of average resistance in waves compared to calm water. This phenomenon is also discussed. The work closes with the conclusions and future work proposals.

2. State-of-the-art and the methodology

Experiments with FWTs have been crucial for the conceptual development, and to validate the numerical models necessary to face their design. In particular, the Offshore Code Comparison (OC) and DeepCwind initiatives, involving experiments in MARIN (see, among others, Gueydon and Weller [16]; Robertson et al. [17] have been significant for this aim. However, these experiments have referred to the moored conditions, whereas the focus of this study is on towing operations, with possible presence of waves.

Regarding towing dynamics, the most relevant aspect is to assess resistance and motions. In towing conditions it is also important to pay attention to the possibility of instability of in-line towing and to the possibility of occurrence of fishtailing (e.g. Refs. [18–22]).

As for resistance of blunt bodies, the literature is limited. Blight and Dai [23] conducted a systematic experimental research with barges. Apart from the hull geometric similarity with a quasi-prismatic platform, they share similar draft-length ratios, which becomes important when a floating wind turbine is designed to be towed from standard harbors that usually impose draft limitations. Other important references are the ones that model the resistance due to bow waves. Dagan and Tulin [24,25] created a model for the contribution to resistance due to two-dimensional bow waves, providing estimates of the added drag for high Froude numbers (based on the draft). A more general approach in terms of the bow geometry was developed by Trinh and Chapman [26], but they did not provide estimates of the added drag. An additional set of relevant references are those dealing with added resistance in waves of blunt bodies. Ohkusu [27] modeled the added resistance of blunt bow ships in very short waves. Their research is interesting, but restricted to that kind of waves, compared to longer ones in present study. There are other works on this topic [28,29], but the

geometries dealt with are radically different from the present platform, which makes their results inapplicable. Accordingly, presently available literature does not seem to provide sufficient information with reference to the floating structure addressed in the present study.

When it comes to the transport and towing of floating wind turbines, the literature is scarce. Bachynski and Moan [30] remarked that one of the presented alternatives in their work had the static stability to allow for its tow-out to the installation site. Myland et al. [10] succinctly documented the resistance in calm water and waves of one of the versions of the GICON concept, also a TLP floater. Amate et al. [9] discussed the use of an auxiliary system for transporting the TLPWIND (see Ref. [31]) design. Both Myland et al. [10] and Amate et al. [9] provided sufficient information to perform some quantitative comparisons with the present concept, a task that aims at providing a wider perspective about the hydrodynamics of the TLP concept studied in this work. Recently, Cardoso et al. [32] have conducted a computational analysis of the transport phase of a free-float capable innovative design for offshore wind turbines.

Concerning the added resistance in waves, discussions are available on topics such as the scaling of the results and methods of defining test matrices (see, e.g. Ref. [33]), but none specifically focus on blunt bodies such as FWTs. Finally, risk of excessive motions associated with the dynamic stability issues while towing in waves is another critical topic that is not addressed in the present literature. This problem will be also treated herein by measuring the motions of the platform during tests carried out in relevant wave conditions for the towing operation.

Considering the discussion above, this paper will investigate resistance in calm water and in waves, as well as motions, for a floating offshore wind turbine platform during towing operations.

The study presented in the paper addresses a free-float capable TLP intended to support a state-of-the-art 10 MW turbine on the basis of a series of experimental tests. The study provides information on resistance in calm water and in waves, as well as comparisons with similar results from the, actually limited, existing literature on the subject. Tests in waves are also carried out in order to assess platform motions in different sea states.

3. Description of the prototype platform, tower, and the turbine assembly

The details of CENTEC-TLP with the 10 MW Turbine were presented in Uzunoglu and Guedes Soares [13], and detailed information regarding the design methodology is available in Uzunoglu and Guedes Soares [34,35]. A summary of these works, including the turbine and the tower is provided below.

The upwind three-bladed turbine was designed by DTU

(Technical University of Denmark) as a 10 MW unit [15] that results from a revised up-scaling of NREL's 5 MW reference turbine [36]. The main particulars of the wind turbine are reported in Table 1.

The tower's details and the rotor nacelle assembly are in Tables 2 and 3. Combining them results in the mass data in Table 4 and places the structure's center of gravity at 85.9 m above the water level. These are the most relevant data for the towing tests since they affect the overall dynamic behavior of the structure. The presence of the rotor also causes a 32 cm offset in of the center of gravity in the longitudinal direction.

Table 5 lists the sizes of the platform components. Some fundamentals on the terminology regarding offshore platforms may help to understand the geometry better. As shown in Fig. 2, pontoons are the horizontal components (e.g., a cylindrical pontoon resembles a tree log in water). When vertical, they are termed "columns" as in the definition of semisubmersibles (i.e., a column-stabilised unit as in Ref. [37]). For example, heaving cylindrical columns have their waterplane area constant while it varies for cylindrical pontoons.

The CENTEC-TLP is designed to float on its pontoons in a manner similar to a semisubmersible in transport. Its waterplane area is designed to have large moment of inertia to increase the meta-centric radius and, thus, provide stability. The overall length and the beam of the platform are 49 m, with the lower columns having 10.5 m sides. The lower and upper columns are prismatic and feature rounded corners using a diameter close to $D/6$, where D is the prismatic column's side length. According to Chakrabarti [38], arrangements close to this corner radius do not lead to any disadvantages compared to cylindrical structures regarding hydrodynamics. The lower and upper columns follow that recommendation. The pontoons, on the other hand, are arranged to be rectangular. This pontoon geometry has an advantage over cylindrical alternatives: the waterplane area stays constant as the structure heaves. Therefore, they are adjusted to aid in the overall stability of the platform. The mass data of this configuration is in Table 6.

In its free-floating condition, the platform has a GM value of 27.76 m, at a mean draft of 3.85 m. The shallow draft is deliberate; it allows towing the platform without being concerned with shore-side depth limits. Floaters with higher drafts have issues similar to spar platforms: although they are stable, they cannot be towed to location. When free-floating, there is a static inclination angle resulting from the longitudinal offset in the turbine and tower's center of gravity. Numerically, this value corresponds to a 0.22-degree static pitch.

While being towed and when installed, the structure needs to avoid ending in wave resonance. DNVGL recommends avoiding 5 to 25-s wave excitation ranges [39]. However, waves above 20 s generally reflect conditions that correspond to storms and harsh weather. Since towing operations are carried out only where the weather window allows it, limiting this range to 5–20 s (i.e., omitting severe weather conditions) is possible. The platform natural periods are 4.8 s for heave, and 22.3 s for pitch, where pitching is more of a concern in terms of stability. The elasticity of the tower was not considered in the numerical model's initial estimation. Since a pitching period that goes beyond 20 s is

Table 1
Specifications of the DTU 10 MW turbine.

Parameter	Value	Units
Rated power	10	[MW]
Hub height	129	[m]
Rotor mass	227962	[kg]
Nacelle mass	446036	[kg]

Table 2
Mass details of the tower model and the moments of inertia about its centre of gravity.

Parameter	Value	Units
Tower mass	628442	[kg]
I _{xx}	6.52E+08	[kg · m ²]
I _{yy}	6.52E+08	[kg · m ²]
I _{zz}	7.84E+06	[kg · m ²]
Centre of gravity	[0, 0, 57.5]	[m, m, m]

Table 3
Mass details of the rotor nacelle assembly.

Parameter	Value	Units
Total mass	673998	[kg]
Centre of gravity	[0.61, 0, 131.56]	[m, m, m]

Table 4
Mass details of the tower, rotor, and the nacelle combination.

Parameter	Value	Units
Total mass	1302440	[kg]
Centre of gravity	[0.32, 0, 85.9]	[m, m, m]
Inertia about the X axis	2.43E+09	[kg · m ²]
Inertia about the Y axis	2.45E+09	[kg · m ²]
Inertia about the Z axis	2.24E+07	[kg · m ²]
1st fore-aft natural period	4.00	[s]

Table 5
Platform's design variables.

Parameter	Value	Units
Height, L (from keel to nacelle top)	149.0	[m]
Overall length beam, B	49.0	[m]
Pontoon side length	4.0	[m]
Lower column corner radius	2.1	[m]
Lower column height	7.5	[m]
Lower column side length	10.5	[m]
Height of the central column above the waterline	10.0	[m]
Distance between the keel and the pontoons	1	[m]
Installation depth	132	[m]

advantageous and the tower's flexibility lengthens the period [35], this conservative approach was used in the design process of the platform. Accordingly, it is highly probable that the experimental pitching natural frequency stays outside the chosen wave excitation margins since a tower is unlikely to be completely rigid in an experimental setup. Table 7 summarizes these details.

4. Test matrices and experimental setup

4.1. Test matrices

The experimental program included multiple speeds and wave conditions in two towing configurations. With regards to the calm water resistance tests, while towing offshore structures may result in directional instabilities and, consequently, side to side oscillations (fishtailing), lateral displacements were not observed during present experimental campaign. Additionally, some screening experiments with initial lateral offsets were carried out, and the rectilinear path was quickly established. As a consequence, though the matter deserves a further study of various factors (e.g., the cable length), these variations were not considered a priority at this stage and were left for future work.

Tests were carried out both in regular and irregular waves

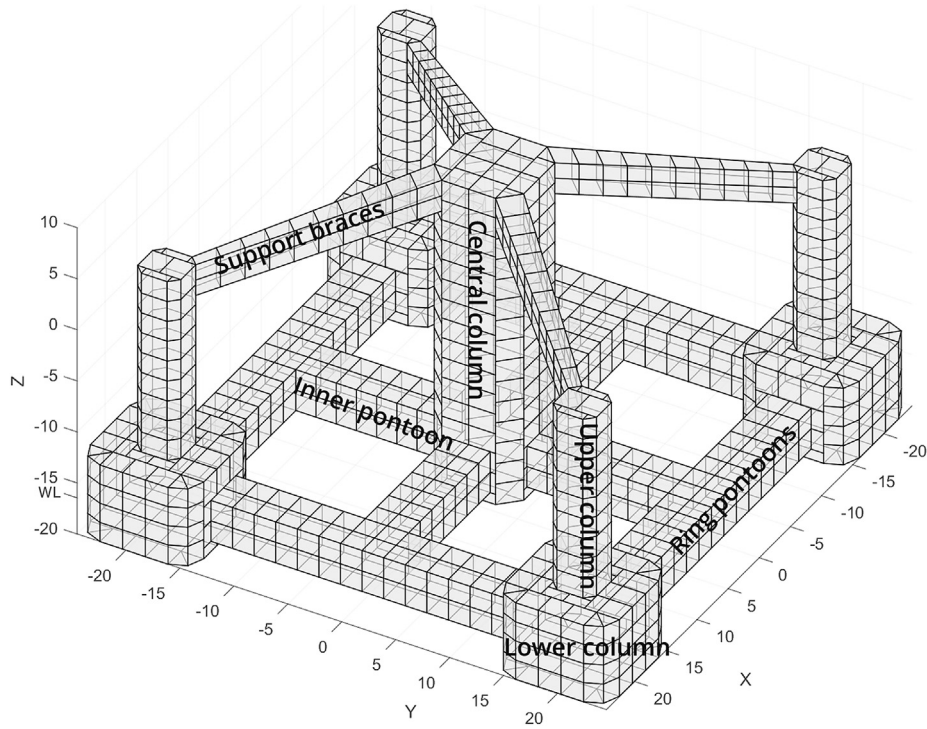


Fig. 2. The platform components and the reference system.

Table 6
Platform's mass data.

Parameter	Value	Units
Mass	2208.6	[t]
Centre of gravity measured from the baseline	[0, 0, 8.36]	[m]
Roll inertia	6.90E+08	[kg · m ²]
Pitch inertia	6.90E+08	[kg · m ²]
Yaw inertia	1.04E+09	[kg · m ²]

Table 7
Free-floating condition specifications.

Parameter	Value	Units
GM	27.76	[m]
Mean draft (T)	3.85	[m]
Displacement volume (∇)	3422.4	[m ³]
Static pitch angle (α_5)	0.22	[deg]
Freeboard of the pontoons	1.20	[m]
Wetted surface (S_{BH})	2563.2	[m ²]
Projected frontal area, frontal tow (A_P)	162.5	[m ²]
Projected frontal area, diagonal tow	230.4	[m ²]
Waterplane area, A_W	1127.3	[m ²]
Heave natural period (T_3)	4.70	[s]
Pitch natural period (T_5)	22.3	[s]

Table 8
Wave conditions: single harmonic values for regular waves and significant wave height and peak period for irregular waves.

Wave Set	H/Hs	T/Tp
[-]	[m]	[s]
1	1	7
2	3	10

(Table 8). The 3 m significant wave height (H_s) was considered as an upper limit where towing operations can be safely undertaken. This value coincides with the discussion in Santos et al. [40], who evaluated the possibility of raising the limit to 3 m from 1.5 m for personnel and equipment transfer to offshore wind turbines. The significant wave height of 1 m was taken as the second test condition.

[41,42] present several scatter diagrams for areas around the Iberian peninsula for which the Levelized Cost of Energy (LCOE) has been found to be good [43,44]. Out of this data, Galicia was selected as the testing environment where the most probable spectral peak periods (T_p) for the two selected significant wave heights (i.e., 1 m and 3 m) approximately correspond to 7 and 10 s. The same wave height (H) and period (T) combinations were also selected to test regular waves (i.e., 1 m at 7 s and 3 m at 10 s). This information is

Table 9
Experimental test matrix.

Set id.	Wave condition	Speed [kn]	Tow config.	Tow pts.	Wave setup
1	Calm water	1	frontal	2	[-]
2	Calm water	2	frontal	2	[-]
3	Calm water	3	frontal	2	[-]
4	Regular waves	2	frontal	2	1, 2
5	Irregular waves	2	frontal	2	2
6	Irregular waves	3	frontal	2	1
7	Calm water	1	diagonal	1, 2	[-]
8	Calm water	2	diagonal	1, 2	[-]
9	Calm water	3	diagonal	1, 2	[-]
10	Calm water	4	diagonal	1, 2	[-]
11	Calm water	5	diagonal	1, 2	[-]
12	Calm water	6	diagonal	1, 2	[-]
13	Regular waves	2	diagonal	1, 2	1, 2
14	Regular waves	5	diagonal	1, 2	1, 2
15	Irregular waves	2	diagonal	1, 2	2
16	Irregular waves	3	diagonal	1, 2	1
17	Irregular waves	5	diagonal	1, 2	1, 2

summarized in Table 8. The wave conditions are examined in 6 speeds, describing 12 encounter frequencies.

The complete set of experiments are summarized in Table 9, listing speeds up to 6 knots on various environmental and towing scenarios. The wave sets and the speeds are self-explanatory. The towing configuration defines whether the platform was pulled from one or two towing line connection points. The wave setup relates to the information in Table 8. Similar setups are grouped into sets to keep the table concise. For instance set number 14 describes four tests. The platform is towed in regular waves, at 5 knots, using the 45-degree configuration. This setup is repeated using one and two towing points, for both wave definitions (i.e., 1 and 2) given in the previous Table 8, in a total of four tests.

The connection points were selected so that the towing cables do not intersect the platform's components (e.g., a connection at the upper columns may cause the towing lines to connect to the tug at an angle that will cause friction at the edges of the lower columns) and stay parallel to the water. Furthermore, the cables should do not get submerged into the water during the towing operation. These are issues commonly taken into consideration by tugboat masters. The single-point and two-point configurations are shown in Fig. 3. Along with the zero degree towing case where the pontoons encounter the waves at a right angle, a second configuration rotates the platform 45 deg so that one of the lower columns face the incoming waves. This case is examined to clarify if that configuration is advantageous.

4.2. Experimental setup of the model

The model represented in Fig. 4 was built in composite materials at a 1:60 scale. Since tests with the moored configuration were envisaged, the scaling factor was selected based on the depth of the planned installation site. For the tower, a commercial aluminum bar was chosen, which, together with a weight at the top, allowed to scale the mass, inertia and the first bending mode frequency. A detail of the clamp between the tower and the floater is presented in Fig. 4 and a picture of the entire structure is shown in Fig. 5. Model deviations with respect to prototype are presented in Table 10. The mass deviation is, in reality, a volume error as fixing draft was given priority over the mass value.

Apart from the tower mode, to be later discussed, and the yaw inertia, all deviations are below 5%. ITTC recommendations for free-running tests [45] indicate that GM accuracy should be within 5% (3.6% in this case). Their recommendations for seakeeping tests [46] require displacement deviations to be below 1% (0.6% in this case),

and no specific recommendations are given for inertiae other than adjusting them as best as possible. In this case, deviations in the roll and pitch radii of inertia are below that in the GM.

Regarding the deviation in yaw inertia, the lower columns of the model had to be reinforced due to structural integrity issues, resulting in higher mass in those zones. This deviation in yaw inertia did not represent a hindrance for the current objective since yawing is negligible for the planned experiments. Moreover, as the present campaign and the one with mooring were aimed at providing data for calibrating the numerical model, these modified characteristics of the floater were incorporated as input for the numerical model.

As discussed in section 3, the turbine and blades' weight induces an offset in the x position of the gravity centre (5 mm offset at model scale), which was not considered in the experimental model. However, the associated static tilt angle will still be accounted for when establishing the operational limits in waves later in the paper.

The tower's bending behavior was measured using free decay tests after fixing it to a stable base, and the motions were obtained with several Optitrack markers. An image of the tower bending shape and a PSD of the time history of the tip displacements are provided in Fig. 6. It is seen that the first mode is dominant for which the full scale target period of 4.02s resulted in a 4.72s actual value. This outcome was accepted as modifications of this setup would cause larger errors on the mass, KG, and inertial values.

5. Results

Section 4.1 listed the experimental sets, which comprised calm water conditions along with regular and irregular waves in various towing speeds. The results are provided and discussed in the following sections, and comparisons are given with other TLP transport concepts when applicable. The assessment of towing data for other TLP concepts allows a rapid assessment and comparison of the hydrodynamic performance of the design evaluated in this paper.

In this section, results of calm water and regular waves are discussed first since they provide the main characteristics of the towing resistance and together allow to estimate the added resistance in wave conditions.

5.1. Towing tests in calm water

Since the towing operation is expected to occur in smooth to moderate sea states, resistance tests in calm water are specially

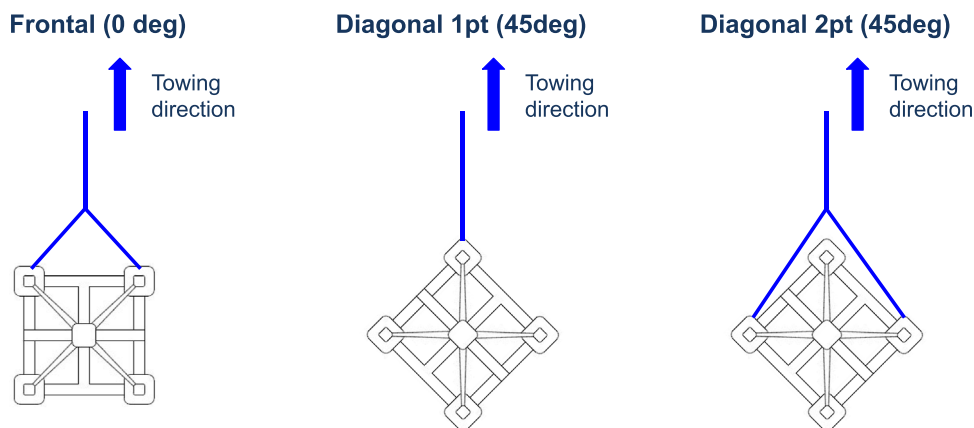


Fig. 3. Towing tests configurations.

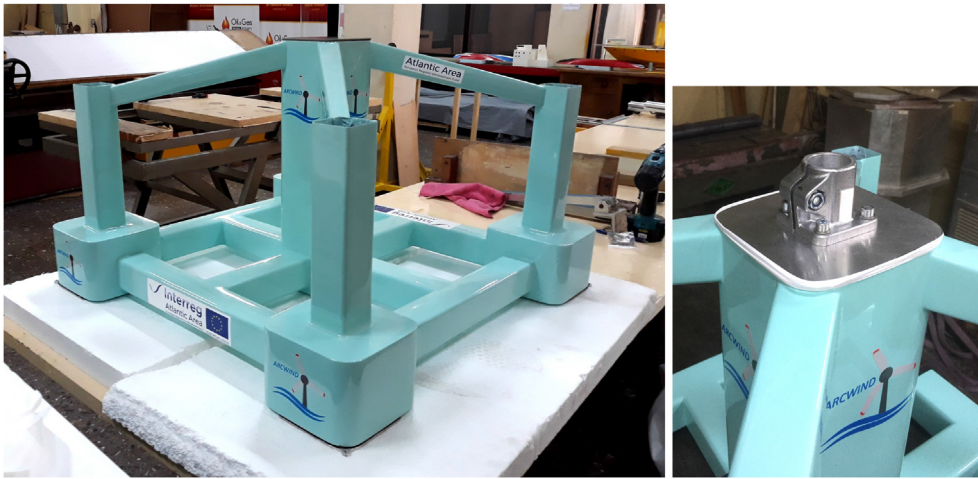


Fig. 4. Model of the floater and detail of the tower base clamp.

important in present research from the quantitative point of view. For this reason, attention has been paid to assess the uncertainty of the resistance tests in calm water. Experimental uncertainties are estimated following the principles and notation of the ITTC General Guideline for Uncertainty Analysis in Resistance Tests [47], taking also into account the example application from Ref. [48]. In order for the narrative of the paper to be kept fluent, such analysis has been included for the interested reader in a dedicated appendix (Appendix A).

A qualitative assessment of the flow around the floater can be appreciated in Fig. 7, for towing speeds equal to 3 and 5 knots for the configuration with diagonal towing from one point (see Fig. 3). The figure is also relevant since the test setup, including the carriage and the towing line, can be appreciated.

When inspecting the free surface downstream of the floater, it is not possible to identify the usual Kelvin wake. A focused view is available in Fig. 8, attesting the presence of a highly non-uniform wake behind the floater.

A disturbance of the free surface due to the presence of a bow wave can be also appreciated with some effort in Fig. 7, with a focused view in Fig. 9. The free surface pattern for the configuration with frontal tow is also characterized by the presence of bow waves, as well as localized disturbances close to the base of the columns (see Fig. 10).

To better understand the effects related to the physical phenomena observed in Fig. 7, Fig. 11 provides a comparison of the experimental drag coefficients, C_D , for different towing tests speeds (i.e., 1, 2, 3, 4, 5 and 6 knots) and configurations (frontal and diagonal with one and two towing points). The included error bars were obtained through the uncertainty analysis described in Appendix A. Drag coefficient notation is used instead of resistance coefficient due to the fact that resistance is mostly due to flow separation:

$$C_D = \frac{R_{cw}}{\frac{1}{2} \rho A_P V^2}. \quad (1)$$

In Eq. (1) R_{cw} is the total resistance, ρ is the water density, V is the speed, and A_P is the projected frontal area (see Table 7), used instead of the wetted surface, as it is customary when the main contribution to the total resistance is the form drag.

The results included in this figure correspond to the averaged forces measured during the towing tests and the three realizations

carried out of each test. The values were normalized using the frontal area of the floater up to the transport draft (see Table 7). The frontal tow configuration projected area was used for all comparisons so that the comparisons in the graphs are useful for selecting among the three options. However, for the sake of completeness, projected frontal areas in both configurations have also been included in Table 7.

Fig. 11 shows that the frontal configuration stands as the one that presents the smallest equivalent C_D for all tested speeds. The results also attest that there appears to be little dependence between the equivalent C_D and speed, indicating almost quadratic dependence of resistance on speed. It is therefore reasonable to assume that the towing resistance of this structure is mainly due to form drag induced by flow separation.

Considering this point, the behavior of the platform is far from that of the barges described by Blight and Dai [23]; whose hydrodynamics shows higher similarity to standard seagoing vessels.

A qualitative comparison of these results with the values proposed in Ref. [49] is relevant. The rounded square section in a frontal flow with reduced corner radius around 0.2 renders $C_D \approx 1.15$ in Ref. [49]. The diamond with rounded corners (type 6 geometry in Ref. [49]) renders $C_D \approx 1.07$ after projecting it on its side (equivalent to using the same projected frontal area in Fig. 11). Both values are similar to the ones obtained in this research for the CENTEC-TLP. The reference values become smaller if they are considered in 3D (~ 0.7) [50], an effect that may be explained here by the large additional wetted surface, which leads to friction and some additional form drag due to the downstream rows of pontoons and lower columns (see Fig. 2).

Returning to the bow wave, its resulting additional contribution to resistance may help to explain the small relative differences between the coefficients obtained for towing speeds higher than 3 kn compared to those for lower speeds (see Fig. 11) for the diagonal configurations. In a different context (two-dimensional flow, high Froude number based on the draft and low based on length) [24,25] showed the bow wave induced drag coefficient to have a slow growth, being proportional to the 2/3 power of the Froude number based on the length. The physics is herein more complex, but this result may give an idea of the effects in place.

To extrapolate the value to full scale, the drag coefficient will be assumed to be equal to the model scale. This approach is justified on the basis that the drag is the sum of form drag, which scales with

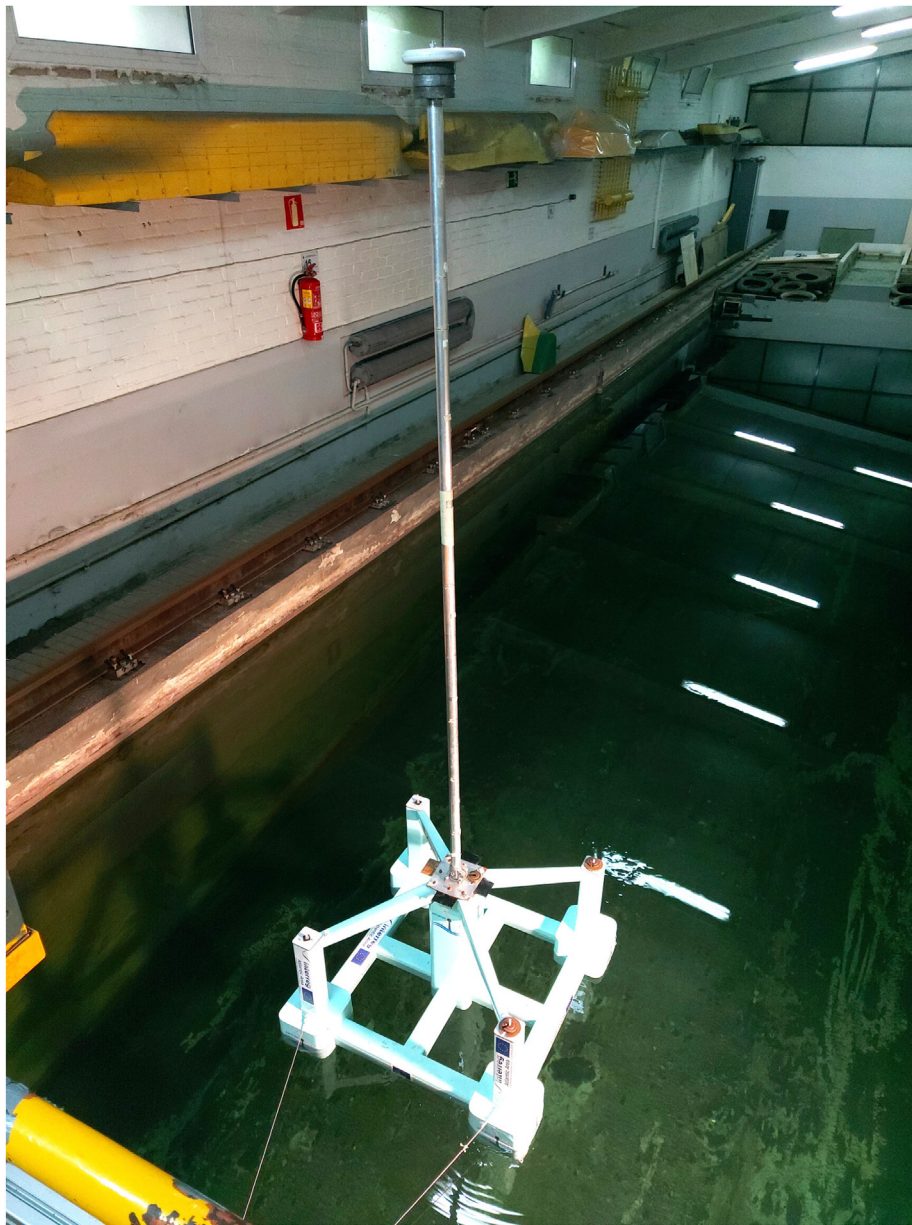


Fig. 5. Model with the tower.

Table 10

Model parameters and deviations. r_x , r_y , r_z are the inertia radii in the respective axes (see Fig. 2).

Parameter	Prototype	Model	deviation [%]
Mass [kg]	3511040	16.160	0.6
$[XG, YG, ZG]/B$	[0.006, 0, 0.581]	[0,0,0.56]	[-0.3.6]
GM/B	0.527	0.504	3.60
r_x/D	0.445	0.432	2.92
r_y/D	0.446	0.433	2.91
r_z/B	0.353	0.406	14.91
1st fore-aft natural period [s]	4.00	0.61	18.0

the square of the velocity, and the bow wave resistance, whose force coefficient is a function of the Froude number (equal for the model and the prototype).

Considering this point, results regarding the estimated full scale resistance per unit designed wind turbine power are provided in

Fig. 12. The data shown in this figure corresponds to the set of experiments 1–3 and 7–12 in Table 9.

Fig. 12 also includes the results obtained using the transport concepts for FWTs provided in Refs. [9,10]. The towing resistances of these concepts are referred in the figure as 2.3 MW-TLP and 5 MW-TLP, respectively. The results obtained for the 2.3 MW-TLP include the towing configuration. This figure includes the error bars for the results of the present concept, but they can not be observed in the actual figure as the absolute value of the related uncertainties is negligible.

The data shows that the concept assessed during the current experimental campaign stands as a solution with lower normalized towing resistance than the ones provided in the literature for the 2.3 MW-TLP and 5 MW-TLP designs. Considering the geometry of the 2.3 MW-TLP floater (a number of separated low diameter vertical cylinders), and the combined form of the 5 MW-TLP platform and barge, a possible explanation is that their larger towing

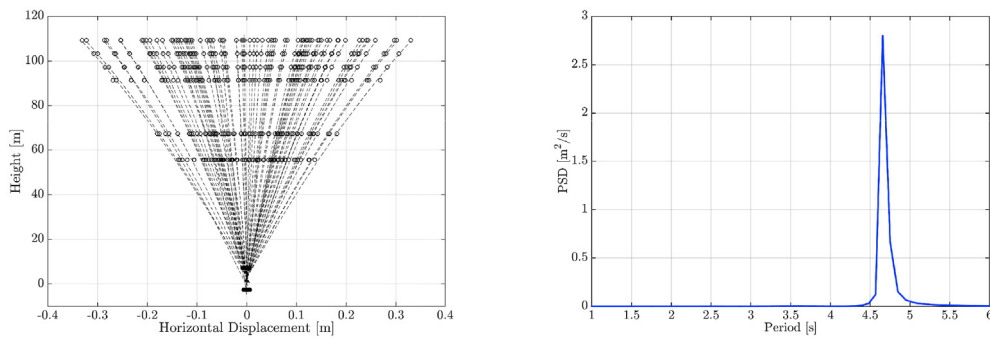


Fig. 6. Tower bending test. Deformed shapes (left) and tip motion spectrum (right).

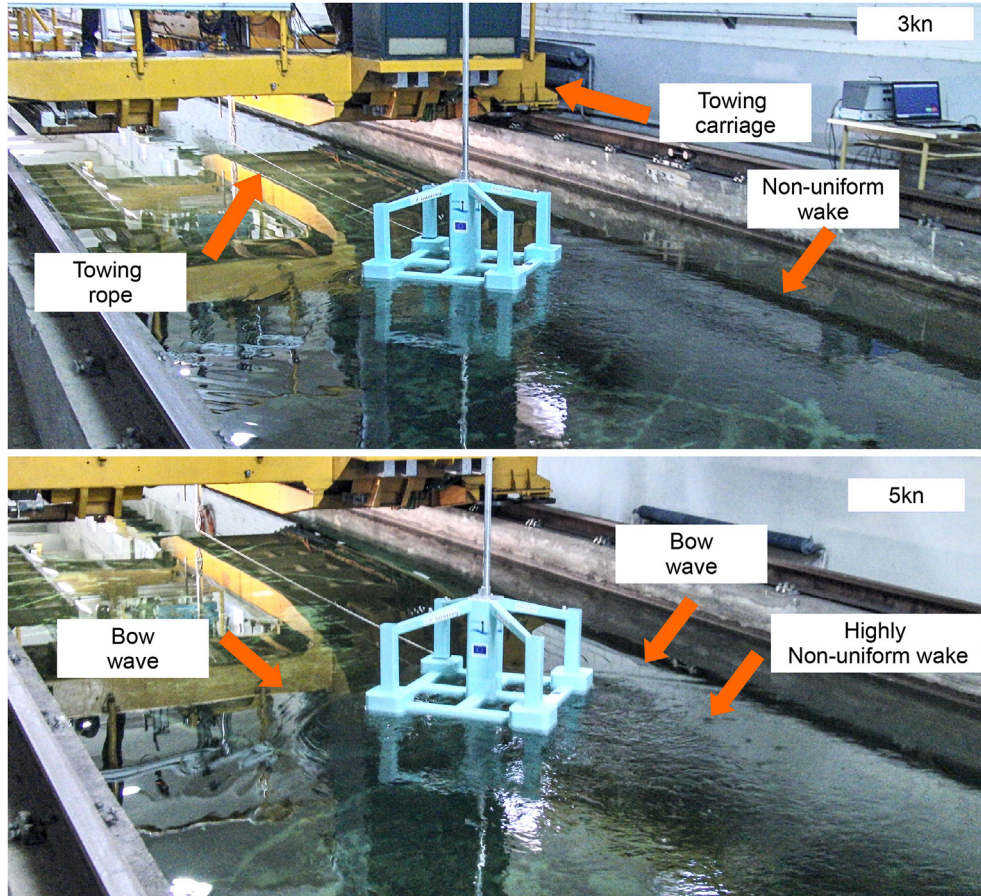


Fig. 7. Diagonal towing from one point (see Fig. 3): free surface patterns for towing speeds equal to 3 knots (top) and 5 knots (bottom).

resistance, when compared to the present design, may be related to a substantially larger form drag.

The relevance of this comparison, in the context of this work, is not limited to the assessment of the hydrodynamic performance of the present design within the existing results in the literature, but also provides a background for the development of models to estimate the Levelized Cost of Energy (LCOE) of offshore wind farms (see e.g. Feng and Shen [51] and Lerch et al. [52]). These models aim to provide an estimation of the capital cost of the project per installed kilowatt and they stand a research topic that has received increasing attention over the last years. This complementary evaluation is also provided for the estimated towing resistance in waves in the following sections.

5.2. Towing tests with waves

5.2.1. Added resistance in regular waves

The normalized added resistance in waves for the CENTEC-TLP and 2.3 MW-TLP concepts is given in Fig. 13 and Fig. 14 for the towing configurations. The averaged added resistance in waves was obtained by subtracting the measured resistance in calm water conditions from the total towing resistance measured in waves. Vertical axes of these figures provide the added resistance in waves, normalized by the turbine power and the square of wave amplitude, and the x-axis presents the wave period.

Added resistance in waves for the diagonal towing is significantly lower than for the frontal towing. Moreover, negative results

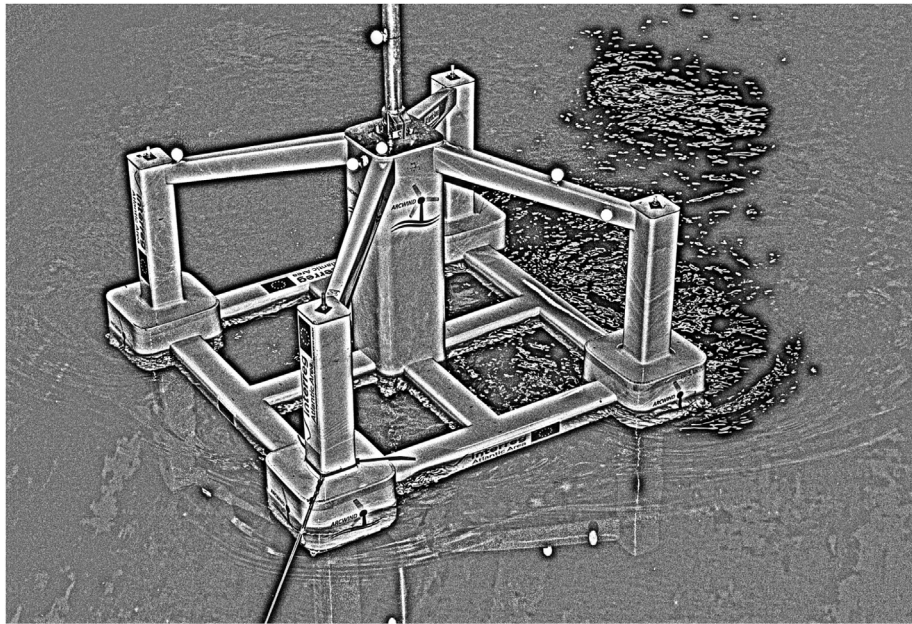


Fig. 8. Diagonal towing from one point (see Fig. 3): wake for towing speed equal to 5kn.

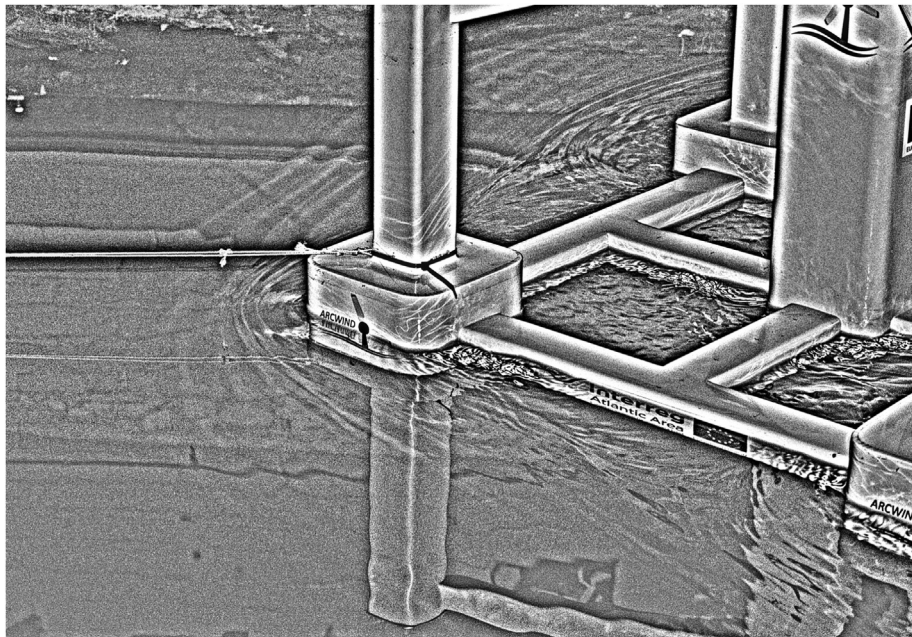


Fig. 9. Diagonal towing from one point (see Fig. 3): bow wave for towing speed equal to 5kn.

for the normalized added resistance in waves were obtained with the CENTEC-TLP in several cases. This is a result for which no reference in the literature has been found. The hypothesis formulated here is that, in these encounter frequencies, the harmonic pressure field resulting from the waves may reduce separation, and, eventually, the total resistance component associated to separation effects. Also, an additional effect may arise from the interaction of the incident wave with the moonpool-type opening that exists between the inner and the ring pontoons of the platform base (see Fig. 2). Considering the peculiarity of the observed phenomenon, a dedicated appendix (Appendix B) has been included presenting a repeatability analysis, aiming at assessing the obtained results

accounting for estimated experimental uncertainty.

Overall, the negative added resistance in waves measured in the diagonal towing configuration results in a lower total towing resistance when compared with the frontal towing configuration. The cases with low T_w (see Fig. 14) present larger variability between 1 and 2 points towing if compared with the case with $T_w = 10s$, which displays similar added resistance for both diagonal towing configurations.

Results in Fig. 13 show that, for the frontal towing configuration, the added resistance in waves is significantly lower than for the 2.3 MW-TLP concept, even though a more detailed comparison, with the same speeds, would be necessary. Results for the diagonal

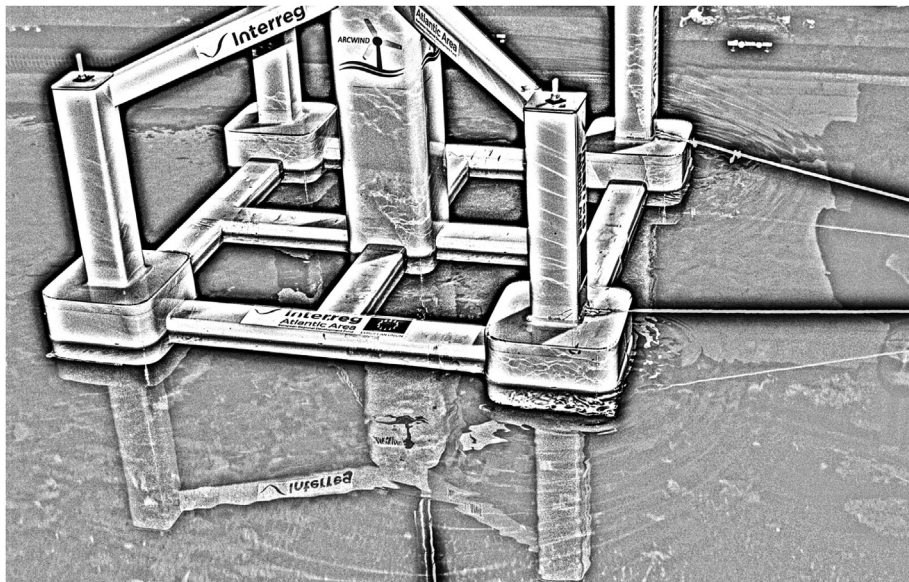


Fig. 10. Frontal tow from one point (see Fig. 3): bow wave for towing speed equal to 3kn.

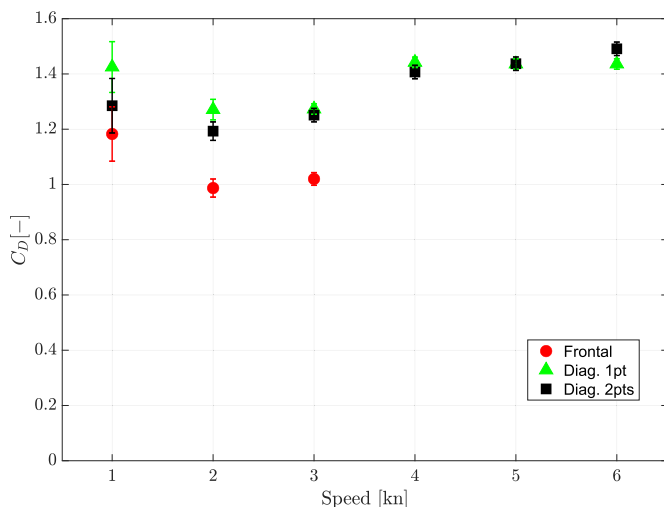


Fig. 11. C_D for towing speeds equal to 1, 2, 3, 4, 5 and 6 knots and three different towing configurations.

towing configuration (with comparable speeds), seem to confirm this trend.

5.2.2. Added resistance in irregular waves

Fig. 15 shows the normalized added resistance in irregular wave conditions. The normalized values were obtained with the same approach used for regular waves, but substituting A with $H_s/2$ and taking T_w equal to the peak period of each sea condition.

Frontal towing configurations show similar behavior in both regular and irregular wave conditions, with positive added resistances. Results provided in Fig. 15 also attest that the added resistance in irregular waves is characterized by negative values in some cases, when the diagonal configuration is adopted.

Similarly to regular waves (see Fig. 14), in irregular waves (Fig. 15) one can observe that for the sea conditions with peak period equal to 10s, the resistance obtained for both towing configurations (i.e. 1 and 2 points) shows similar normalized added resistances.

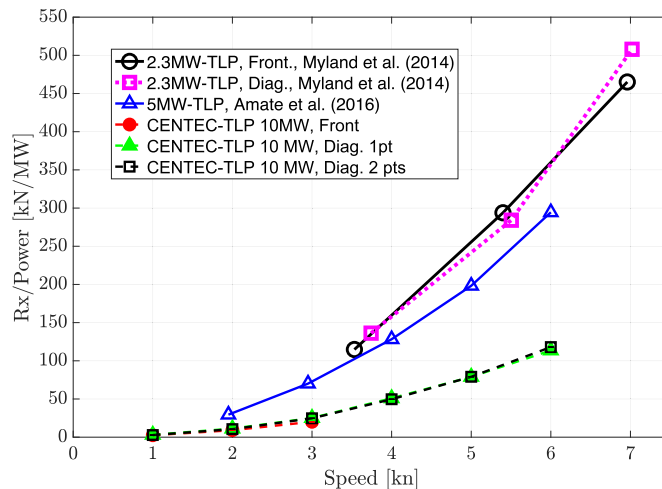


Fig. 12. Comparison of the total towing resistance in transport of different FWT concepts.

For the sake of illustration of the magnitude of the added resistance in waves, assume that the CENTEC-TLP platform is being towed at a speed equal to 2 kn in a sea state characterised with a peak period corresponding to 10s and significant wave height of 3m. From the results provided in Fig. 15, it is possible to estimate that the added resistance in waves is equal to 77 kN, while the resistance measured for this towing condition in calm water conditions is equivalent to 100 kN (see Fig. 12). Therefore, the added resistance is of the same order of magnitude as the resistance measured in calm water conditions (i.e. it corresponds to approximately 44% of the total resistance measured in waves). The tugboat necessary for this operation would be of the 20 tonnes range, a quite affordable one.

5.3. Motions in waves

5.3.1. Motions in waves during transport

The motion responses RMS values provided in Figs. 16 and 17

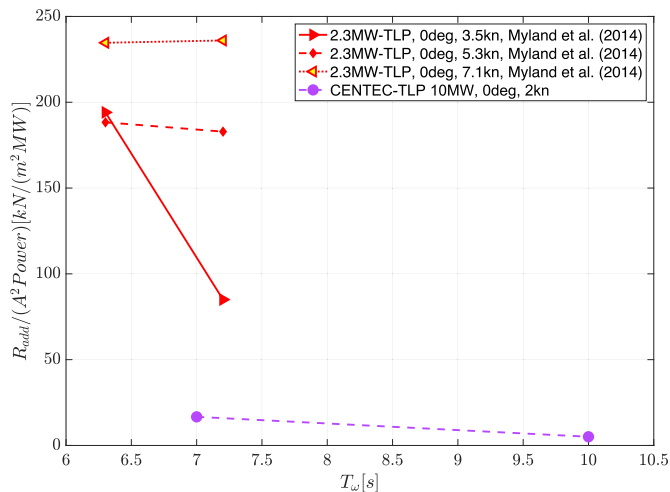


Fig. 13. Added resistance in regular waves measured with the frontal towing configuration.

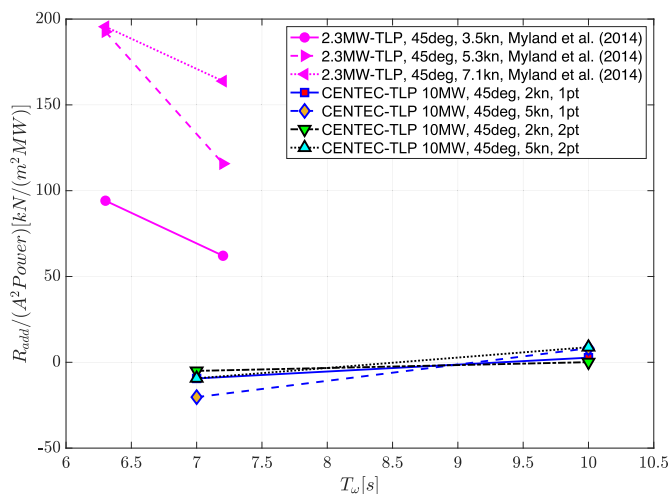


Fig. 14. Added resistance in regular waves measured with the diagonal towing configuration.

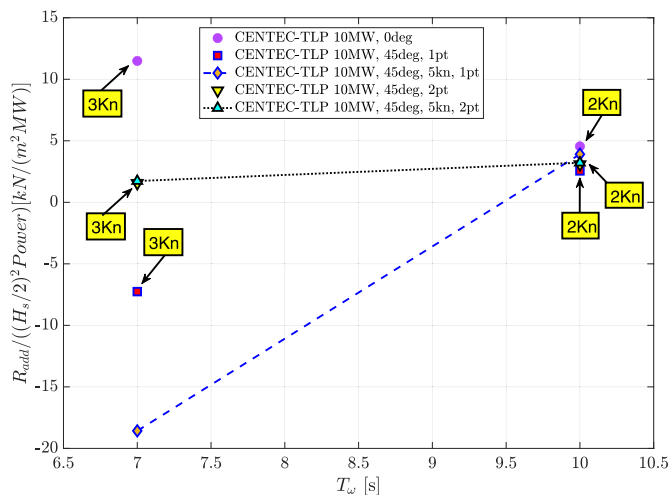


Fig. 15. Added resistance in irregular waves measured with the diagonal towing configuration.

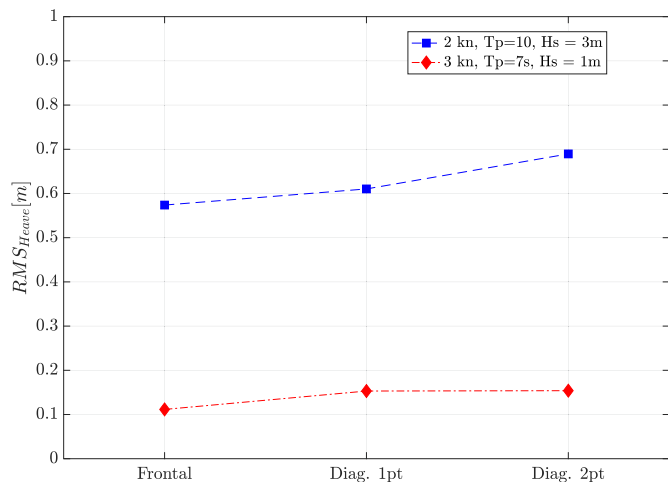


Fig. 16. Measured Heave RMS values.

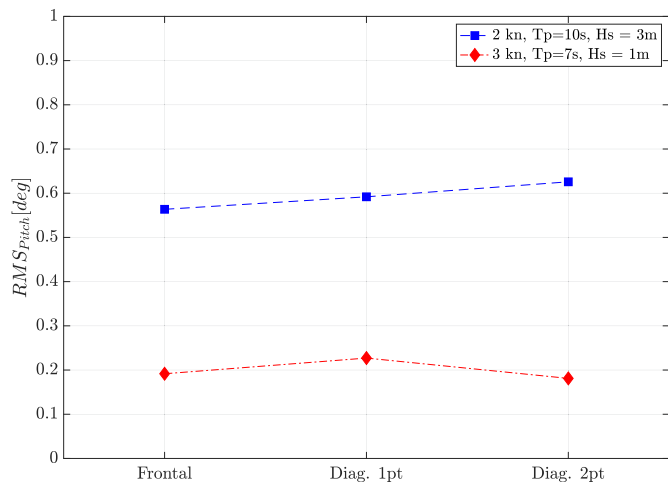


Fig. 17. Measured Pitch RMS values. Maximum static tilt angle equal to 10deg.

illustrate the dynamic behaviour of the floater in waves during transport. The heave responses in the sea conditions tested are characterized by remarkable low RMS values.

Pitch motions are also characterized by small RMS values, in this case of the order of 0.7 deg. Therefore, if the static tilt angle is taken into account (0.2 deg) the platform always shows lower responses than the maximum admissible static angle of 10 deg. Similar dynamic behaviour of the pitch motions is expected for both towing conditions and, therefore, it results in limited differences between the measured RMS pitch responses.

Observing the results of the two sea states studied, one can estimate the maximum expected value for the pitch angle to be around 2.25 deg (4 times the RMS times 0.93), for sea states with H_s less or equal than 3m and T_p less or equal than 10s, and for the three towing configurations. This value is relatively far from the maximum admissible tilt angle (equal to 10deg). According to the scatter diagram in Refs. [41,42], used to design this platform, the selected peak periods correspond to the most probable ones for $H_s = 1m$ and $H_s = 3m$. However, a better characterization of the pitch dynamics is necessary for a rigorous extrapolation to a complete wave scatter diagram for the location of the transport operation. Additionally, other limits such as personnel and tugboat capabilities will also be of concern despite being outside the scope

of this study.

5.3.2. Free floating: decay tests

An additional brief discussion regarding the decay tests is included, since they provide information about the natural frequencies of the motions as well as damping characteristics of the system, the latter being crucial information for the numerical modelling of this type of floaters. For each discussed motion (i.e. heave, roll and pitch), tests with different initial amplitudes were carried out.

Damping effects close to the resonance periods of the motions assessed in this study are usually governed by non-linearities. This case is mainly due to the fact that these systems are subjected to weak potential damping effects. Therefore, it is expected that large motions may appear when the resonances of the system are excited and, under these conditions, non-linearities dominate the responses. In this work, damping was quantified following the approach provided in Faltinsen [53]; which involves the linearisation of the non-linear drag effects.

Fig. 18 provides some illustrative results for pitch, roll and heave

motions. In this figure, the graphs on the left show the time series for the pitch, roll and heave motions, respectively. The graphs on the right show the estimated linear damping ratio values for different motions amplitudes.

The mean natural periods for the pitch and roll motion show, as expected, a very close agreement ($T_{pitch} = 27.8s$ and $T_{roll} = 27.7s$). These results are larger than the ones estimated numerically, which are provided in Table 7. Longer experimental pitch periods were expected as the numerical model did not take the elasticity of the tower into account, leading to a stiffer structure (see main dynamic characteristics included in section 3). The slight differences between the measured periods of the pitch and roll motions are related to the experimental uncertainties.

Towing operation of the platform will be carried out in calm sea states, which present small amounts of energy close the resonances of the pitch and roll motions. Therefore, a representative value equal to 1% of the critical damping can be adopted for these degrees of freedom (DOFs). Decay tests for the heave motion show that the heave undamped natural period is equal to 4.49s (full scale). Assuming, small amplitude heave responses and taking into

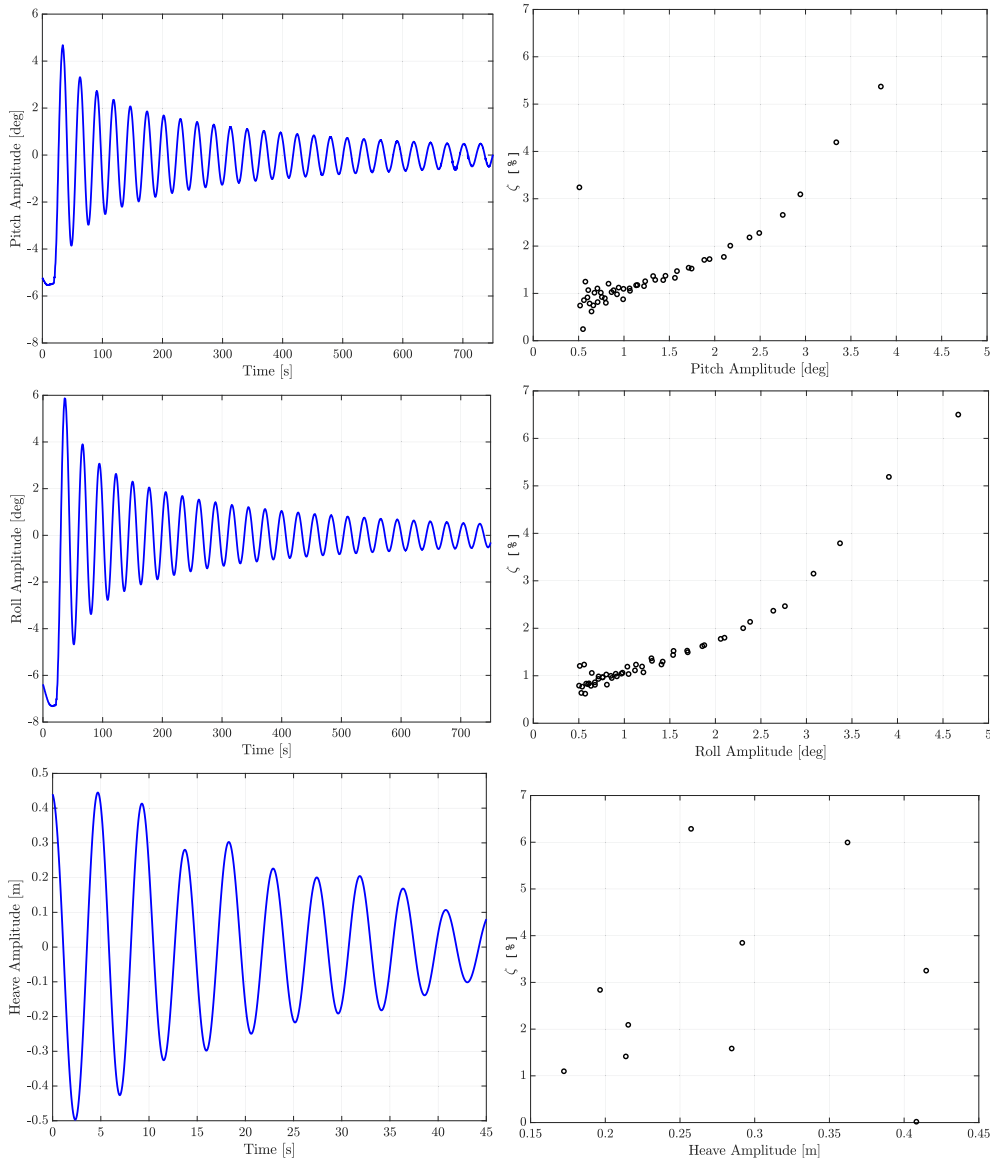


Fig. 18. Decay time series and linear damping ratio for pitch (top), roll (middle) and heave (bottom) motions.

Table 11

Natural periods and linear damping ratios measured for the heave, roll and pitch motions.

Mode	Model Period [s]	ζ [%]
Heave	4.49	2%
Roll	27.73	1%
Pitch	27.80	1%

account the decay measurements for the heave motions, the damping coefficient can be set equal to 2% of the critical damping.

Table 11 summarizes the estimated natural period for the heave, roll, and pitch motions as well as the equivalent linear damping ratio, ζ . Estimated experimental linear damping values are in accordance with the predicted estimations provided in Ref. [35].

6. Conclusions

Results of towing tests of a state-of-the-art tension leg platform (CENTEC-TLP) supporting a 10 MW floating wind turbine in calm water and waves have been presented and discussed. Regarding the similarities between the present floating wind turbine and a barge or blunt bow type vessel in terms of towing resistance, it has been found that the behavior is radically different due to the prevalence of form drag in the present case compared to friction drag for the latter. In what respects to the similarity, in terms of towing resistance, between the present case study and other floating wind turbine designs available in literature, the present design performs significantly better in calm water resistance and comparably well in terms of added resistance in waves. The data corresponding to resistance coefficients and normalized added resistance in waves are provided so that they can serve as reference for future designs. A remarkable outcome of present research is that negative added resistance in waves has been obtained in some of the tests. While this finding deserves further research, the authors hypothesize that the presence of incident waves may partially mitigate separation phenomena. The observed behavior of resistance in waves poses some conceptual difficulties in using standard spectral techniques for estimating added resistance in irregular waves starting from regular sea results. A comprehensive study of this topic would therefore be an interesting continuation of the presented research. For the chosen representative sea states (significant wave height and peak period) and towing speeds, measured responses attest that the pitch motions are always significantly lower than the maximum admissible static angle. Heave responses also show remarkable low RMS values for all towing tests configurations assessed.

It is hoped that this research could be useful for studies on the hydrodynamics of transport operations of novel floating wind turbine designs. In addition, the obtained results may hopefully set the grounds for further investigations on specific aspects of particular interest, such as the observed negative added resistance in waves, and, more generally, the complex hydrodynamics of bluff bodies advancing in waves.

CRedit authorship contribution statement

Jordi Mas-Soler: Conceptualization, Investigation, Writing – original draft, Writing – review & editing, Visualization. **Emre Uzunoglu:** Conceptualization, Writing – original draft, Writing – review & editing, Visualization. **Gabriele Bulian:** Methodology, Validation, Investigation, Writing – original draft, Writing – review & editing, Visualization. **C. Guedes Soares:** Conceptualization, Writing – review & editing, Funding acquisition. **Antonio Souto-Iglesias:** Conceptualization, Methodology, Validation, Writing –

original draft, Writing – review & editing, Visualization, Supervision, Funding acquisition.

Declaration of competing interest

The authors declare that they have no known competing financial interests or personal relationships that could have appeared to influence the work reported in this paper.

Acknowledgments

The authors acknowledge the funding received from the ARC-WIND project “Adaptation and Implementation of Floating Wind Energy Conversion Technology for the Atlantic Region (EAPA 344/2016)” which is co-financed by the European Regional Development Fund (ERDF) through the Interreg Atlantic Area Programme. The project was also supported by the Spanish Ministry for Science, Innovation and Universities (MCIU) under grant RTI2018-096791-B-C21 “Hidrodinámica de elementos de amortiguamiento del movimiento de aerogeneradores flotantes”. This work contributes to the Strategic Research Plan of the Centre for Marine Technology and Ocean Engineering (CENTEC), which is financed by the Portuguese Foundation for Science and Technology (Fundação para a Ciência e Tecnologia - FCT) under contract UIDB/UIDP/00134/2020. The authors would also like to thank Juan Luis Chacón, Leonardo Diaz Gutiérrez, Antonio Medina Manuel and Cristina Romero Monte for their help during the experimental campaign.

Appendix A. Notes on experimental uncertainty in calm water tests

Uncertainty studies in experimental hydrodynamics of floating wind turbines are scarce. Robertson et al. [54] did a referential work on the topic, focusing on assessing whether the uncertainty of the second order effects measured in experiments for moored configurations could explain the deviations with respect to a number of numerical models. This work had as precursor a previous one co-authored by these authors [55], in which the main sources of uncertainty in this type of campaigns had been identified. Another important reference in the field is due to Desmond et al. [56], who investigated the impact on experimental uncertainty of introducing aerodynamic and rotor gyroscopic loading on a model multirotor floating wind energy platform during physical testing.

The present work deals with the free-floating configuration not in moored condition but during the transport phase, being therefore more connected to the ITTC works on uncertainty of resistance tests than to the previously referred works. Indeed, the analysis is herein conducted in accordance to the ITTC recommendations as presented in the general principles in Ref. [57] and the example corresponding to the total resistance coefficient documented in Ref. [58].

It has been shown in the bulk of the paper that resistance is mostly due to separation. For this reason, the resistance coefficient has been referred as the drag coefficient (eq. (1)) and its uncertainty is assessed to define the size of the error bars in Fig. 11.

Following the ITTC general principles [57], the uncertainty in C_D is obtained by propagating that of the variables involved in its data reduction formula, with the proportionality coefficients being the partial derivatives with respect the corresponding variable, i.e:

$$u^2(C_D) = \left(\frac{2}{\rho V^2 A_p} \right)^2 u^2(R_{cw}) + \left(\frac{-4R_{cw}}{\rho V^3 A_p} \right)^2 u^2(V) + \left(\frac{-2R_{cw}}{\rho V^2 A_p^2} \right)^2 u(A_p)^2. \quad (\text{A.1})$$

The contribution of density is neglected, as its own uncertainty, including its corresponding factor, is negligible (see Refs. [48,58] for comparable examples in which this is the case).

In order to better understand the procedure to estimate these terms, consider the particular case of the lowest speed (1kn) and the frontal tow as an example.

Regarding the uncertainties in the forces, they are classified as A (repetition related) and B (calibration) types, and assumed independent, leading to:

$$u^2(R_{cw}) = u_A^2(R_{cw}) + u_B^2(R_{cw}). \quad (\text{A.2})$$

The A-type uncertainty is obtained from analyzing the repeatability of the experiments, estimated from repeated measurements using the expression [47]:

$$u_A(R_{cw}) = \frac{\sigma}{\sqrt{N_{cw}}}, \quad (\text{A.3})$$

with σ being the standard deviation of mean resistance obtained from each repeated test, and N_{cw} the number of repeated calm water tests. Even though the estimate for σ is poor with low N_{cw} , in our particular case we decided to have three tests for all cases with $V \leq 3$ kn, instead of a particular case with a larger number of repetitions. This procedure has the advantage of having estimates for σ for a larger number of cases. The values obtained for σ are in any case tiny, indicating high repeatability and therefore removing concerns in regards to this approach.

Following [47], the standard deviation is obtained using the classic unbiased discrete estimator:

$$\sigma = \sqrt{\frac{1}{N_{cw} - 1} \sum_{j=1}^{N_{cw}} \left(R_{cw} - R_{cw}^j \right)^2}, \quad (\text{A.4})$$

with R_{cw}^j obtained with the mean value (in time) of the resistance, and R_{cw} is the mean value of those R_{cw}^j .

In the particular case of the proposed example, $R_{cw} = 0.116$ N, $\sigma = 1.25 \cdot 10^{-4}$ N, $N = 3$, and therefore $u_A(R_{cw}) = 7.2 \cdot 10^{-5}$ N.

As for the B-type uncertainty for the resistance, a one component load-cell was used for the measurements, whose calibration was verified prior to the tests. The standard deviation of the residuals is taken as the $u_B(R_{cw})$ uncertainty:

$$u_B(R_{cw}) = 0.0053 \text{ N}. \quad (\text{A.5})$$

Therefore, applying Eq. (A.2), one gets $u(R_{cw}) = 0.0053$ N, indicating that calibration is the dominant factor.

Regarding the uncertainty due to speed, the control system of the carriage renders average velocity values within ± 1 mm/s absolute precision, which, assuming a uniform distribution leads to:

$$u_B(V) = \frac{0.001}{\sqrt{3}} = 5.8 \cdot 10^{-4} \text{ m/s}, \quad (\text{A.6})$$

with $u_A(V) = 5.2 \cdot 10^{-6}$ m/s, obtained analogously to $u_A(R_{cw})$, leading to $u(V) = 5.8 \cdot 10^{-4}$ m/s, with calibration being the main factor.

As for the geometry, the related uncertainty is accounted for through its effect on the projected area, and such uncertainty is obtained from the deviation in volume, ∇ , proportional to that of mass in Table 10. In order to propagate the volume uncertainty on to the projected area's, their dependence on the draft is used (see Tables 5 and 7 for the meaning of the variables involved):

$$u(A_p) = \left| \frac{\partial A_p}{\partial \nabla} \right| u(\nabla) = \left| \frac{\partial A_p / \partial T}{\partial \nabla / \partial T} \right| u(\nabla) = \frac{B}{A_w} u(\nabla) = \frac{0.82}{0.3131} \cdot 0.006 \cdot 0.0163 = 2.54 \cdot 10^{-4} \text{ m}^2. \quad (\text{A.7})$$

This uncertainty aims at accounting for the impact of the deviation (which is unknown within that precision) between the design IGES file and the actual specimen, due to the manufacture tolerances.

Incorporating all individual uncertainties into Eq. (A.1), one gets for the example that $u(C_D) = 0.0582$, with $C_D = 1.1827$, with the main contributor being the uncertainty on the calm water resistance.

The uncertainty $u(C_D)$ is multiplied by a coverage factor $k = 2$ [57], leading to the expanded uncertainty, $U(C_D) = 0.1164$, used to define the size of the error bars in Fig. 11, as indicated at the beginning of this appendix.

The expanded relative uncertainty is therefore.

$$U'(C_D) = \frac{U(C_D)}{C_D} = 0.098 \approx 10\%, \quad (\text{A.8})$$

for the example at hand. This relative uncertainty is directly translated to the predicted full scale calm water resistance in Fig. 12. It is noted, however, that this does not account for uncertainties associated to extrapolation to full scale based on the assumption of equal drag coefficient between model scale and full scale.

The same methodology is applied to every tested speed, leading to the corresponding error bars displayed in Figs. 11 and 12. For the speeds with no repetitions (4–6 knots in diagonal towing), the error bars have been set with the same relative size as those of 3 knots, in principle a conservative value as quantified uncertainties for the considered case tend to reduce as the speed increases, as can be appreciated in Fig. 11 for the cases between 1 and 3 knots.

Appendix B. Further insight into observed reduction of resistance in waves

In order to get more confidence in the obtained results regarding reduction of resistance in waves, an additional experimental campaign was conducted some time (months) after the one discussed in the paper. In between the two campaigns, the model was taken out of the water, and campaigns with other models and objectives were carried out in the tank.

It was decided to focus on the case with diagonal towing from one point, with speed equal to 5kn, regular waves with period $T = 7$ s, wave height $H = 1$ m, for which $R_{add}/(A^2 \text{ Power}) = -20.3$ kN/

(m² · MW) (see Fig. 14). This point belongs to the set 14 in Table 9.

In order to assess the consistency of the results, repeatability was also analyzed for a case with positive added resistance in waves. To this aim, the other point with diagonal tow from one point in set 14, i.e., speed equal to 5 kn, $T = 10s$, $H = 3m$, for which $R_{add}/(A^2 \text{ Power}) = 8.2 \text{ kN}/(\text{m}^2 \cdot \text{MW})$ (see Fig. 14) is also studied.

The results of the repeated tests can be seen in Fig. B.19. As can be clearly appreciated, on the one hand, the case with $H \approx 1m$ presents a consistent reduction in the total resistance when compared the calm water test ($H = 0$), thus suggesting that the added resistance in waves is negative. On the other hand, the case with $H \approx 3m$ shows a consistent larger value than the calm water tests.

Making use of the repetitions in Fig. B.19, an uncertainty assessment can be carried out, aimed at establishing whether one can be confident on the observed negative variation of resistance, taking into account uncertainty bounds. It is noted that uncertainty aspects of measurement of added resistance in waves is a topic for which literature is scarce (see Ref. [59]).

First, as discussed in section 5.2.1, added resistance R_{add} is defined as:

$$R_{add} = R_{Tw} - R_{cw}, \quad (\text{B.1})$$

where R_{Tw} is the total resistance in waves and R_{cw} is the calm water one at the considered speed. If one assumes that the uncertainties in the calm water and wave tests are uncorrelated, one could write:

$$u^2(R_{add}) = u^2(R_{Tw}) + u^2(R_{cw}) \quad (\text{B.2})$$

The total uncertainty of R_{Tw} and R_{cw} can be split in their *A* and *B* type components [57], as done in appendix Appendix A. However, the *B*-type uncertainty, due to load-cell calibration is the same for both measurements, i.e. $u_B(R_{Tw}) = u_B(R_{cw})$ (defined in Eq. (A.5)), which implies that one can write Eq. (B.2) as:

$$u^2(R_{add}) = u_A^2(R_{Tw}) + u_A^2(R_{cw}) + 2 u_B^2(R_{cw}), \quad (\text{B.3})$$

where $u_A(R_{cw})$ and $u_A(R_{Tw})$ for the data available are obtained with the same procedure followed in appendix Appendix A.

With these ideas plus the data in Fig. B.19, one can obtain the terms in Eq. (B.3), to close this appendix reporting $u(R_{add})$ for the two cases considered.

Intermediate and final data are included in Tabs. B.12–B.14, all at model scale.

Table B.12

Uncertainty of calm water resistance for data in Fig. B.19.

R_{cw} [N]	$u_A(R_{cw})$ [N]	$u_B(R_{cw})$ [N]	$u(R_{cw})$ [N]	$U(R_{cw})$ [N]
3.564	0.013	0.0053	0.014	0.028

Table B.13

Uncertainty of total resistance in waves for data in Fig. B.19

T [s]	R_{Tw} [N]	$u_A(R_{Tw})$ [N]	$u_B(R_{Tw})$ [N]	$u(R_{Tw})$ [N]	$U(R_{Tw})$ [N]
7	3.413	0.0220	0.0053	0.023	0.045
10	4.484	0.0101	0.0053	0.011	0.023

Table B.14

Uncertainty of added resistance in waves for data in Fig. B.19. Units for forces are Newtons.

T [s]	R_{Tw} [N]	R_{cw} [N]	R_{add} [N]	$U(R_{Tw})$ [N]	$U(R_{cw})$ [N]	$U(R_{add})$ [N]
7	3.413	3.564	-0.151	0.045	0.028	0.053
10	4.484	3.564	0.920	0.023	0.028	0.036

As one can appreciate, the expanded uncertainty, $U(R_{add})$, for the negative added resistance in wave case is approximately 0.053N, which is smaller in absolute terms than the added resistance in waves for the referred case ($\approx -0.15N$). This provides some confidence that there is actually a reduction of resistance in waves compared to calm water, taking into account both the obtained average results as well as the estimated level of uncertainty, and this topic would deserve a further dedicated research, which is out of the scope of the present one. Similar considerations apply to the case showing a positive added resistance in waves.

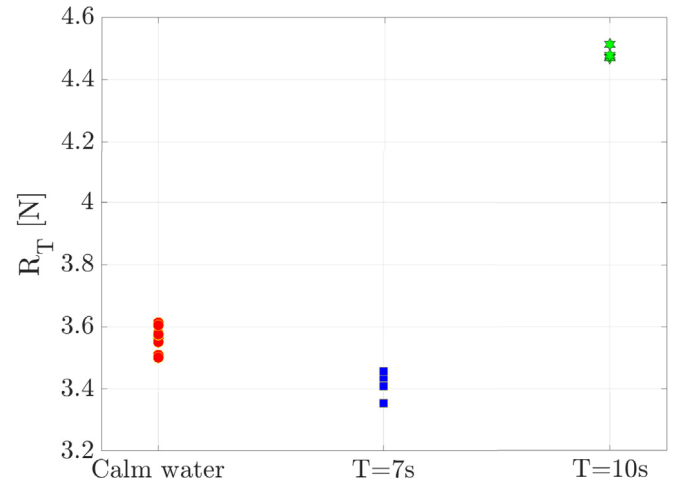


Figure B.19. Model scale total resistance: selected cases in calm water and regular waves with the diagonal towing configuration (towing from one point). $V = 5\text{kn}$ for all cases presented.

References

- [1] H.M. Diaz, C. Guedes Soares, Review of the current status, technology and future trends of offshore wind farms, Ocean. Eng. (2020), <https://doi.org/10.1016/j.oceaneng.2020.107381>.
- [2] Equinor, Floating Offshore Wind in Equinor, 2020. <https://www.equinor.com/en/what-we-do/floating-wind.html>. Online (accessed June 13, 2020).
- [3] S. Rodrigues, C. Restrepo, E. Kontos, R.T. Pinto, P. Bauer, Trends of offshore wind projects, Renew. Sustain. Energy Rev. 49 (2015) 1114–1135, <https://doi.org/10.1016/j.rser.2015.04.092>. ISSN 1364–0321, <http://www.sciencedirect.com/science/article/pii/S1364032115003627>.
- [4] M. Vieira, E. Henriques, M. Amaral, N. Arantes-Oliveira, L. Reis, Path discussion for offshore wind in Portugal up to 2030, Mar. Pol. 100 (2019) 122–131, <https://doi.org/10.1016/j.marpol.2018.11.021>. ISSN 0308–597X, <http://www.sciencedirect.com/science/article/pii/S0308597X18303932>.
- [5] SBM Offshore, Design for Wind Floater Receives ABS Stamp of Approval. <https://www.sbmoffshore.com/news/design-for-wind-floater-receives-abs-stamp-of-approval/>, 2019. Online (accessed June 13, 2020).
- [6] SAIPEM, Hywind-saipem. <https://www.saipem.com/en/projects/hywind>, 2020. Online (accessed June 13, 2020).
- [7] ESTEYCO, ELISA and ELICAN projects. <https://esteyco.com/projects/elisa/>, 2020. Online (accessed June 13, 2020).
- [8] R. Zamora-Rodriguez, P. Gomez-Alonso, J. Amate-Lopez, V. De-Diego-Martin, P. Dinoi, A.N. Simos, A. Souto-Iglesias, Model scale analysis of a TLP floating offshore wind turbine, in: Asme (Ed.), 33rd International Conference on Ocean, Offshore and Arctic Engineering, OMAE, 2014.
- [9] J. Amate, G.D. Sánchez, G. González, Development of a semi-submersible barge for the installation of a TLP floating substructure. TLPWIND® case study, J. Phys. Conf. 749 (sep 2016), 012016, <https://doi.org/10.1088/1742-6596/749/1/012016>.
- [10] T. Myland, F. Adam, F. Dahlias, J. Großmann, Towing tests with the GICON®-TLP for wind turbines, in: 24th International Offshore and Polar Engineering Conference (ISOPE), The International Society of Offshore and Polar Engineers (ISOPE), June 2014.
- [11] B. Kim, T. wan Kim, Scheduling and cost estimation simulation for transport and installation of floating hybrid generator platform, Renew. Energy 111 (2017) 131–146, <https://doi.org/10.1016/j.renene.2017.03.098>. ISSN 0960–1481, <http://www.sciencedirect.com/science/article/pii/S0960148117302902>.
- [12] L. Castro-Santos, V. Diaz-Casas, Life-cycle cost analysis of floating offshore

- wind farms, *Renew. Energy* 66 (2014) 41–48, <https://doi.org/10.1016/j.renene.2013.12.002>, 0, ISSN 0960–1481, <http://www.sciencedirect.com/science/article/pii/S0960148113006642>.
- [13] E. Uzunoglu, C. Guedes Soares, Hydrodynamic design of a free-float capable tension leg platform for a 10 MW wind turbine, *Ocean. Eng.* 197 (2020) 106888, <https://doi.org/10.1016/j.oceaneng.2019.106888>.
- [14] E. Uzunoglu, C. Guedes Soares, Response dynamics of a free-float capable tension leg platform for a 10 mw wind turbine at the northern iberian peninsula, in: C. Guedes Soares (Ed.), *Developments in Renewable Energies Offshore*, UK Taylor and Francis, London, 2021, pp. 408–416.
- [15] C. Bak, F. Zahle, R. Bitsche, K. Taeseong, A. Yde, L.C. Henriksen, A. Natarajan, M.H. Hansen, Description of the DTU 10 MW Reference Wind Turbine, Technical Report Report-1-0092, DTU Wind Energy, Roskilde, Denmark, 2013.
- [16] S. Gueydon, S. Weller, Study of a floating foundation for wind turbines, *J. Offshore Mech. Arctic Eng.* 135 (3) (June 2013), 031903, <https://doi.org/10.1115/1.4024271>. ISSN 0892–7219.
- [17] F. Wendt, J.M. Jonkman, W. Popko, H. Dagher, S. Gueydon, J. Qvist, F. Vittori, J. Azcona, E. Uzunoglu, C. Guedes Soares, R. Harries, A. Yde, C. Galinos, K. Hermans, J.B. de Vaal, P. Bozonnet, L. Bouy, I. Bayati, R. Bercu, J. Galvan, I. Mendikoa, C.B. Sanchez, H. Shin, S. Oh, C. Molins, Y. Debruyne, OC5 project phase II: validation of global loads of the DeepCwind floating semi-submersible wind turbine, *Energy Procedia* 137 (2017) 38–57, <https://doi.org/10.1016/j.egypro.2017.10.333>. ISSN 1876–6102, <http://www.sciencedirect.com/science/article/pii/S1876610217352931>, 14th Deep Sea Offshore Wind R&D Conference, EERA DeepWind/2017.
- [18] M.M. Bernitsas, N.S. Kekridis, Oscillatory flow around disks and through orifices, *Int. Shipbuild. Prog.* 32 (369) (May, 1985) 112–123.
- [19] M.M. Bernitsas, J.-S. Chung, Nonlinear stability and simulation of two-line ship towing and mooring, *Appl. Ocean Res.* 12 (2) (1990) 77–92, [https://doi.org/10.1016/S0141-1187\(05\)80032-X](https://doi.org/10.1016/S0141-1187(05)80032-X). ISSN 0141–1187, <http://www.sciencedirect.com/science/article/pii/S014111870580032X>.
- [20] E.A. Tannuri, A.N. Simos, A.J.P. Leite, J.A.P. Aranha, Experimental validation of a quasi-explicit hydrodynamic model: fishtailing instability of a single-point moored tanker in rigid-hawser configuration, *J. Ship Res.* 45 (4) (2001).
- [21] A. Fitriyadi, H. Yasukawa, Course stability of a ship towing system, *Ship Technol. Res.* 58 (1) (2011) 4–23, <https://doi.org/10.1179/str.2011.58.1.001>.
- [22] M. Sinibaldi, G. Bulian, Towing simulation in wind through a nonlinear 4-dof model: bifurcation analysis and occurrence of fishtailing, *Ocean. Eng.* 88 (2014) 366–392, <https://doi.org/10.1016/j.oceaneng.2014.06.007>. ISSN 0029–8018, <http://www.sciencedirect.com/science/article/pii/S0029801814002200>.
- [23] G. Blight, R. Dai, Resistance of offshore barges and required tug horsepower, in: *10th Offshore Technology Conference*, OTC, 1978, pp. 2345–2352.
- [24] G. Dagan, M. Tulin, Bow Waves before Blunt Ships. Technical Report, Office of Naval Research, Tech. Report 117.14, 1969.
- [25] G. Dagan, M.P. Tulin, Two-dimensional free-surface gravity flow past blunt bodies, *J. Fluid Mech.* 51 (3) (1972) 529–543, <https://doi.org/10.1017/S0022112072002344>.
- [26] P.H. Trinh, S.J. Chapman, The wake of a two-dimensional ship in the low-speed limit: results for multi-cornered hulls, *J. Fluid Mech.* 741 (2014) 492–513, <https://doi.org/10.1017/jfm.2013.589>.
- [27] M. Ohkusu, Added resistance of blunt bow ships in very short waves, *J. Kansai Soc. Nav. Archit. Jpn.* 202 (1986) 39–42. The Japan Society of Naval Architects and Ocean Engineers.
- [28] W. Duan, C. Li, Estimation of added resistance for large blunt ship in waves, *J. Mar. Sci. Appl.* 12 (1) (2013) 1–12.
- [29] K.-K. Yang, Y. Kim, Numerical analysis of added resistance on blunt ships with different bow shapes in short waves, *J. Mar. Sci. Technol.* 22 (2) (2017) 245–258.
- [30] E.E. Bachynski, T. Moan, Design considerations for tension leg platform wind turbines, *Mar. Struct.* 29 (1) (2012) 89–114, <https://doi.org/10.1016/j.marstruct.2012.09.001>. ISSN 0951–8339, <http://www.sciencedirect.com/science/article/pii/S0951833912000627>.
- [31] E. Oguz, D. Clelland, A.H. Day, A. Incecik, J.A. López, G. Sánchez, G. González-Almeria, Experimental and numerical analysis of a TLP floating offshore wind turbine, *Ocean. Eng.* 147 (2018) 591–605, <https://doi.org/10.1016/j.oceaneng.2017.10.052>. ISSN 0029–8018, <http://www.sciencedirect.com/science/article/pii/S0029801817306649>.
- [32] J. Cardoso, M. Vieira, E. Henriques, L. Reis, Computational analysis of the transportation phase of an innovative foundation for offshore wind turbine, 0(0), *Ships Offshore Struct.* (2020) 1–10, <https://doi.org/10.1080/17445302.2020.1779016>.
- [33] S. Liu, A. Papanikolaou, G. Zaraphonitis, Prediction of added resistance of ships in waves, *Ocean. Eng.* 38 (4) (2011) 641–650, <https://doi.org/10.1016/j.oceaneng.2010.12.007>. ISSN 0029–8018, <http://www.sciencedirect.com/science/article/pii/S0029801810002775>.
- [34] E. Uzunoglu, C. Guedes Soares, Parametric modelling of marine structures for hydrodynamic calculations, *Ocean. Eng.* 160 (2018) 181–196, <https://doi.org/10.1016/j.oceaneng.2018.04.049>.
- [35] E. Uzunoglu, C. Guedes Soares, A system for the hydrodynamic design of tension leg platforms of floating wind turbines, *Ocean. Eng.* 171 (2019) 78–92, <https://doi.org/10.1016/j.oceaneng.2018.10.052>.
- [36] J. Jonkman, S. Butterfield, W. Musial, G. Scott, Definition of a 5MW Reference Wind Turbine for Offshore System Development. Technical Report NREL/TP-500-38060, National Renewable Energy Laboratory (NREL), Golden, CO, USA, 2009.
- [37] DNV, DNV-RP-C103, Column-Stabilised Units, Technical report, Hovik, Norway, 2012.
- [38] S. Chakrabarti, *Handbook of Offshore Engineering (2-volume Set)*, first ed., Elsevier, 2005. ISBN 978-0-08-044381-2.
- [39] DNVGL, Global Performance Analysis of Deepwater Floating Structures, *DNVGL-RP-F205*. DNV GL AS, 2017.
- [40] T.A. Santos, E. Carichas, N. Fonseca, J. Pessoa, F. Duarte, J. Abreu Valente, L. Baptista, J. Cruz, M. Leal, Development of an integrated system for personnel and equipment transfer to offshore wind turbines, in: C. Guedes Soares, Y. Garbatov, S. Sutulo, T.A. Santos (Eds.), *Maritime Engineering and Technology*, Taylor & Francis Group, London, 2012, pp. 631–645, <https://doi.org/10.1201/b12726-87>. ISBN 9780415621465.
- [41] D. Silva, A.R. Bento, P. Martinho, C. Guedes Soares, High resolution local wave energy modelling in the Iberian Peninsula, *Energy* 91 (2015a) 1099–1112, <https://doi.org/10.1016/j.energy.2015.08.067>.
- [42] D. Silva, A.R. Bento, P. Martinho, C. Guedes Soares, Corrigendum to High resolution local wave energy modelling in the Iberian Peninsula [Energy 91 (2015) 1099–1112], *Energy* 94 (2015b) 857–858, <https://doi.org/10.1016/j.energy.2015.08.067>.
- [43] L. Castro-Santos, D. Silva, A.R. Bento, N. Salvação, C. Guedes Soares, Economic feasibility of floating offshore wind farms in Portugal, *Ocean. Eng.* 207 (2020b) 107393, <https://doi.org/10.1016/j.oceaneng.2020.107393>. ISSN 0029–8018, <http://www.sciencedirect.com/science/article/pii/S0029801820304224>.
- [44] L. Castro-Santos, A.R. Bento, D. Silva, N. Salvação, C. Guedes Soares, Economic feasibility of floating offshore wind farms in the north of Spain, *J. Mar. Sci. Eng.* 8 (1) (2020a), <https://doi.org/10.3390/jmse8010058>. ISSN 2077–1312, <https://www.mdpi.com/2077-1312/8/1/58>.
- [45] ITTC, International Towing Tank Conference, Recommended Procedures and Guidelines: Free Running Model Tests, Report 7.5-02-06-01. Technical Report, 2014.
- [46] ITTC, International Towing Tank Conference, ITTC Quality System Manual, Recommended Procedures and Guidelines, Procedure: Seakeeping Experiments, Report 7.5-02-07-02.1. Technical Report, 2017.
- [47] ITTC, International Towing Tank Conference, General Guideline for Uncertainty Analysis in Resistance Tests, Report 7.5-02-02-02. Technical Report, 2014.
- [48] ITTC, International Towing Tank Conference, Recommended Procedures and Guidelines: Example for Uncertainty Analysis of Resistance Tests in Towing Tanks, Report 7.5-02-02-02.1. Technical Report, 2014.
- [49] DNV, Recommended Practice, DNV-RP-C205, Environmental Conditions and Environmental Loads. Technical Report, Det Norske Veritas, Høvik, Norway, 2007.
- [50] H. Sakamoto, M. Arie, Flow around a cubic body immersed in a turbulent boundary layer, *J. Wind Eng. Ind. Aerod.* 9 (3) (1982) 275–293, [https://doi.org/10.1016/0167-6105\(82\)90020-4](https://doi.org/10.1016/0167-6105(82)90020-4). ISSN 0167–6105, <http://www.sciencedirect.com/science/article/pii/0167610582900204>.
- [51] J. Feng, W.Z. Shen, Design optimization of offshore wind farms with multiple types of wind turbines, *Appl. Energy* 205 (2017) 1283–1297. ISSN 0306–2619, <http://www.sciencedirect.com/science/article/pii/S0306261917311285>.
- [52] M. Lerch, M. De-Prada-Gil, C. Molins, G. Benveniste, Sensitivity analysis on the leveled cost of energy for floating offshore wind farms, *Sustainable Energy Technologies and Assessments* 30 (2018) 77–90. ISSN 2213–1388, <http://www.sciencedirect.com/science/article/pii/S2213138818301486>.
- [53] O.M. Faltinsen, *Sea Loads on Ships and Offshore Structures*, Cambridge University Press., Cambridge, UK, 1990. ISBN 0521372852, <http://www.loc.gov/catdir/toc/cam031/90043346.html>.
- [54] A. Robertson, E.E. Bachynski, S. Gueydon, F. Wendt, P. Schunemann, Total experimental uncertainty in hydrodynamic testing of a semisubmersible wind turbine, considering numerical propagation of systematic uncertainty, *Ocean. Eng.* 195 (2020) 106605, <https://doi.org/10.1016/j.oceaneng.2019.106605>. ISSN 0029–8018, <http://www.sciencedirect.com/science/article/pii/S0029801819307309>.
- [55] A. Robertson, E.E. Bachynski, S. Gueydon, F. Wendt, P. Schunemann, J. Jonkman, Assessment of experimental uncertainty for a floating wind semisubmersible under hydrodynamic loading, in: ASME (Ed.), *37th International Conference on Ocean, Offshore and Arctic Engineering (OMAE)*, 2018.
- [56] C. Desmond, J.-C. Hinrichs, J. Murphy, Uncertainty in the physical testing of floating wind energy platforms: accuracy versus precision, *Energies* 12 (3) (Jan 2019) 435, <https://doi.org/10.3390/en12030435>. ISSN 1996–1073.
- [57] ITTC, International Towing Tank Conference, Guide to the Expression of Uncertainty in Experimental Hydrodynamics, Report 7.5-02-01-01, Revision 02. Technical Report, 2014.
- [58] ITTC, International Towing Tank Conference, ITTC Quality System Manual, Recommended Procedures and Guidelines, Guideline to Practical Implementation of Uncertainty Analysis, Report 7.5-02-01-07, Technical report, 2017a.
- [59] D.-M. Park, J. Lee, Y. Kim, Uncertainty analysis for added resistance experiment of kvlc2 ship, *Ocean. Eng.* 95 (2015) 143–156, <https://doi.org/10.1016/j.oceaneng.2014.12.007>. ISSN 0029–8018, <http://www.sciencedirect.com/science/article/pii/S0029801814004648>.